Strong Exciton-Photon Coupling and lasing behavior in

All-Inorganic CsPbBr₃ Micro/nanowire Fabry-Pérot cavity

Wenna Du,[†,#] Shuai Zhang,[†,‡,#] Jia Shi [†,‡] Jie Chen,[†,‡] Zhiyong Wu,[†] Yang Mi,[†] Zhixiong Liu,[⊥] Yuanzheng Li,[†] Xinyu Sui,[†,‡] Rui Wang,[†] Xiaohui Qiu,[†] Tom Wu,[⊥] Yunfeng Xiao,[ℓ,] Qing Zhang,[§,*] and Xinfeng Liu[†,‡,*]*

[†]Division of Nanophotonics, CAS Key Laboratory of Standardization and Measurement for Nanotechnology, CAS Center for Excellence in Nanoscience, National Center for Nanoscience and Technology, Beijing 100190, P. R. China

[‡]University of Chinese Academy of Sciences, Beijing 100049, P.R. China

[§]Department of Materials Science and Engineering, College of Engineering, Research Center for Wide Band Semiconductor, Peking University, Beijing 100871, P. R. China

[⊥]Laboratory of Nano Oxides for Sustainable Energy, Material Science and Engineering (MSE), King Abdullah University of Science & Technology (KAUST), Thuwal, 23955-6900, Saudi Arabia

[ℓ]State Key Laboratory for Mesoscopic Physics, Collaborative Innovation Center of Quantum Matter, School of Physics, Peking University, Beijing 100871, China

[#]Wenna Du and Shuai Zhang contributed equally to this work.

*Email address: liuxf@nanoctr.cn, q_zhang@pku.edu.cn and yfxiao@pku.edu.cn

Contents of the Supporting Information:

Note1: Chemical vapor deposition (CVD) and characterization of $CsPbBr_3$ nanowires

Note2: Spatially resolved PL and propagation loss spectrum of $CsPbBr_3$ nanowire

Note3: Confirmation of Fabry-Pérot cavity mode

Note4: Fitting of exciton binding energy

Note5: The exciton-polariton model and fitting of the dispersion curve

Note6: Numerical calculations of coupling strength

Note7: Mode simulation and effective volume of $CsPbBr_3$ nanowire waveguide

Note8: Group index of a $CsPbBr_3$ nanowire modeled with different coupling strength

Note9: Temperature-dependent study of Rabi splitting energy

Note10: Power dependent lasing energy blueshift

Table 1: Oscillator strengths of different semiconductor materials

Note1 Chemical vapor deposition and characterization of CsPbBr$_3$ nanowires

Commercially available PbBr$_2$ (power, 99.999%) and CsBr (powder, 99.999%) were purchased from Sigma Aldrich. These materials were used without any further purification process. 11 mg of PbBr$_2$ and 6.4 mg of CsBr powders (with 1:1 stoichiometry) were placed in the heating center of a quartz tube reactor. The silicon (Si) substrate was positioned at a distance of 12 cm away from the powder source in the downstream. Prior to a deposition, the base pressure of the system was pumped to 10^{-4} Torr after which a 30 sccm of nitrogen was flowed continuously to maintain the pressure at 100 Torr during deposition. The chamber temperature rose from room temperature to the deposition temperature of 575 $^{\circ}$C rapidly in 30 minutes. The deposition process lasted for 10 minutes before the furnace was shut down. The furnace was cooled down to room temperature before the Si substrates were taken out.
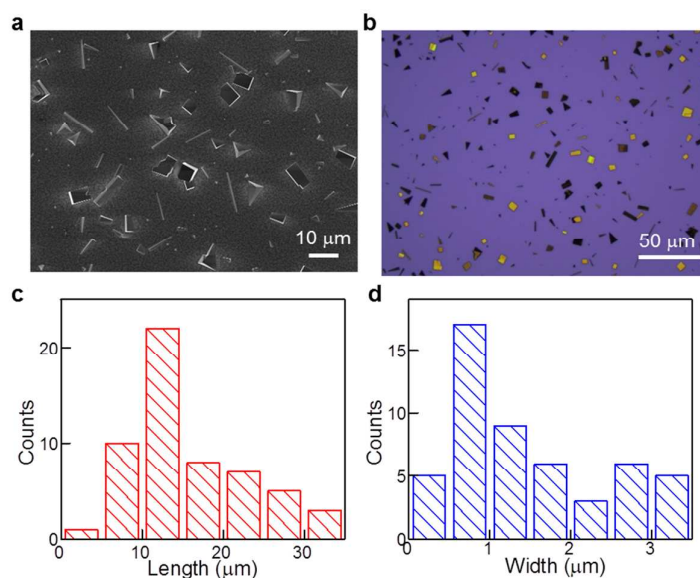

Figure S1| **(a)** Low-magnification SEM and **(b)** optical image of as-grown CsPbBr$_3$ nanostructures. Size distribution statistics for 50 CsPbBr$_3$ nanowires: **(c)** length, **(d)** width.
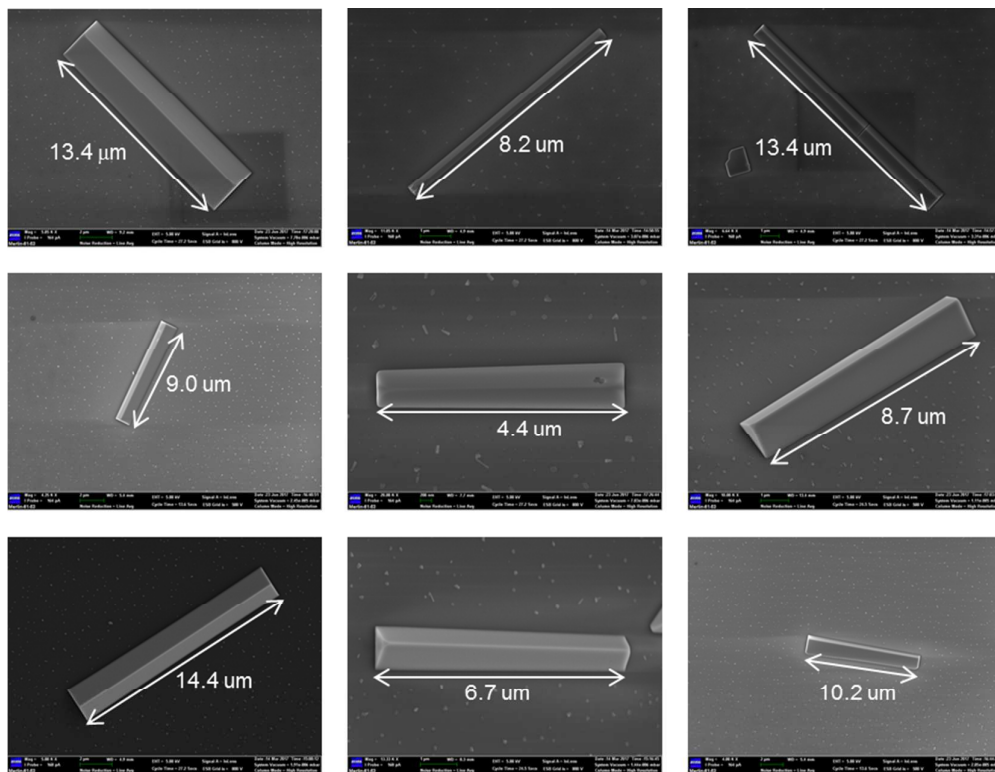
Figure S2| SEM images of CsPbBr$_3$ nanowires with different lengths.

The morphology and structures of the as-grown nanowires were characterized using an optical microscope, AFM in tapping mode, scanning electron microscopy (SEM), X-ray powder diffraction (XRD) in the θ−2θ geometry. From the low/ high-magnification SEM and optical image shown in **Figure S1a-b and S2**, a wide range of CsPbBr$_3$ micro/nanoscale morphologies was produced including nanowires, nanocrystals, and nanoplatelets. The micro/nanowires range in length from 4.4 to 31.7 μm and in width from 0.16 to 3.36 μm (**Figure S1c** and **d**), placing them in an ideal size regime for confining photonic mode in the nanowires and spatial-resolved measurement. Atomic force microscopy (AFM) was used to confirm the cross-section shape and height of the CsPbBr$_3$ nanowires with the lowest optical contrast (**Figure S3**). The height profile (inset) along the yellow dash line reveals the height and the

width of a CsPbBr$_3$ nanowire. Statistical results of several nanowires' AFM show that height-to-width ratios are almost same for all the nanowires and are around 2.4. The AFM data also show that the roughness of the CsPbBr$_3$ nanowires is very small (<1 nm). This demonstrates the CsPbBr$_3$ nanowires with a highly smooth surface are perfectly flat in optical level and little surface defects.
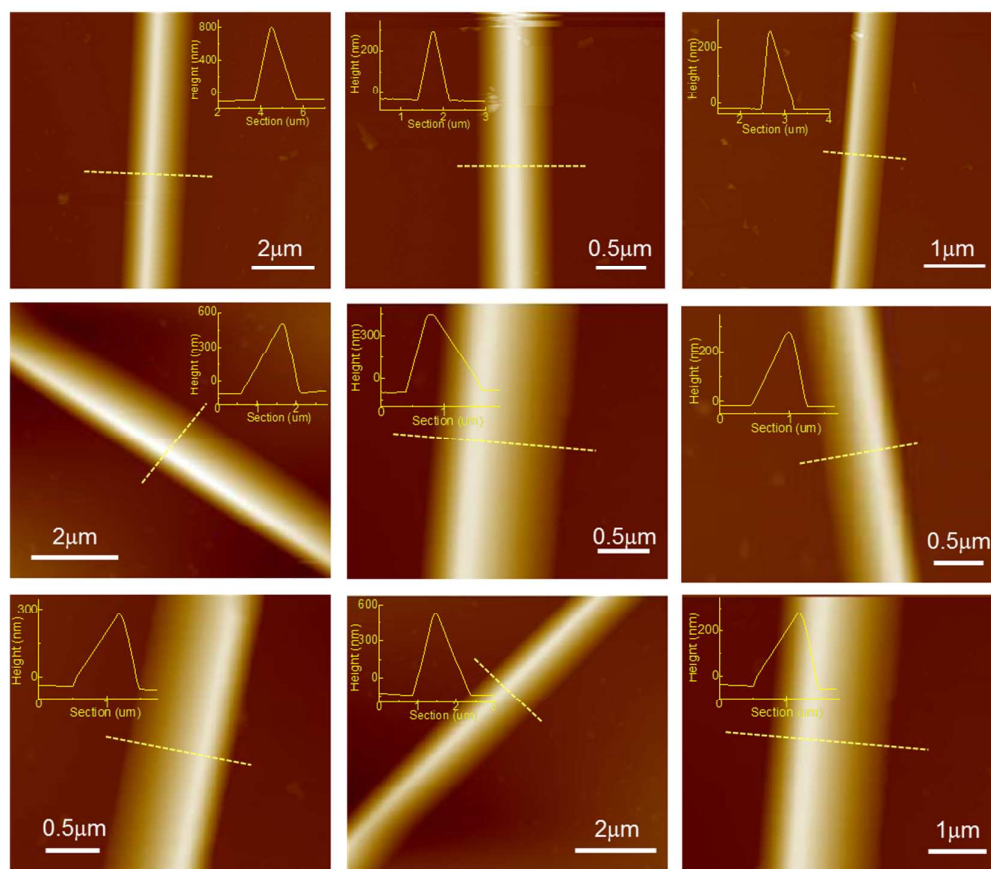

Figure S3| AFM image of CsPbBr$_3$ nanowires and height profile along the yellow dash line.

CsPbX$_3$ are known to crystallize in orthorhombic, tetragonal, and cubic polymorphs of the perovskite lattice with the cubic phase being the high-temperature state for all compounds.[1-3] Interestingly, we find that CsPbBr$_3$ nanowires crystallize in the cubic phase, which can be attributed to the combined effect of the high synthesis

temperature and contributions from the surface energy.[2, 4-5] The X-ray diffraction (XRD) pattern of the $CsPbBr_3$ nanowires shows strong diffraction peaks which can be assigned to the cubic crystal structure, and does not contain impurity peaks from either the PbI_2 or CsBr starting materials (**Figure S4a**). The nanowire composition was determined by energy-dispersive X-ray spectroscopy, which indicated the presence of Cs, Pb, and Br in a 0.91:1.0:3.18 ratio, in close agreement with the $CsPbBr_3$ phase (**Figure S4b**).
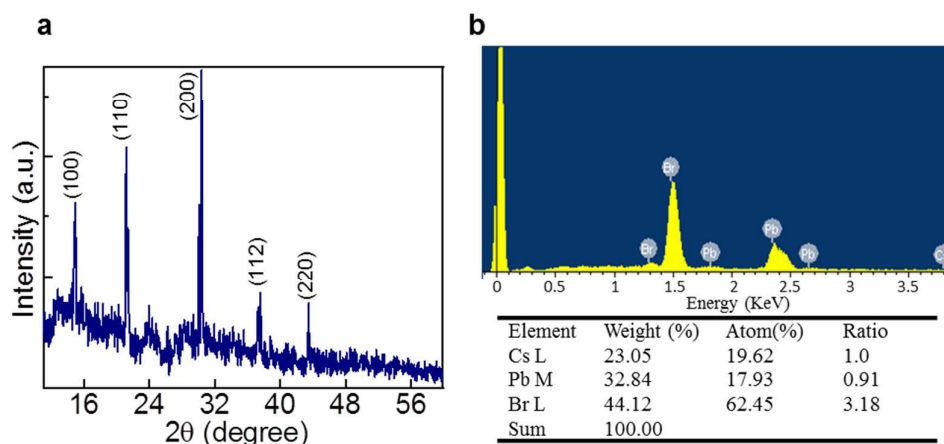

Element	Weight (%)	Atom(%)	Ratio
Cs L	23.05	19.62	1.0
Pb M	32.84	17.93	0.91
Br L	44.12	62.45	3.18
Sum	100.00		

Figure S4| **(a)** XRD patterns of the as-grown $CsPbBr_3$ micro/nanowires, confirming the cubic crystal structure. **(b)** EDS spectrum from a single-crystalline $CsPbBr_3$ nanowire.

The optical performance of the $CsPbBr_3$ nanowires is exhibited in **Figure S5** which presents the absorption spectrum (blue line) and photoluminescence (PL) (green line). The absorption onset at ~527 nm (2.35 eV) is observed in the absorption spectrum of $CsPbBr_3$ perovskite nanowires, which corresponds to the optical band gap as previous reported.[6-9] The PL from single $CsPbBr_3$ perovskite nanowire is centered at ~531 nm (2.34 eV) with a narrow full width at half maximum (FWHM) of 15 nm (66 meV), Stokes-shifted by 13 nm (57 meV) with respect to the excitonic absorption peak
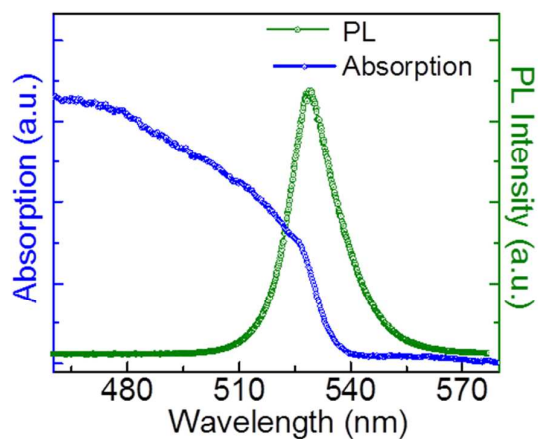
(**Figure S5**).

Figure S5| Room temperature PL and absorption spectra of $CsPbBr_3$ nanowire. Blue trace, the absorption spectrum of $CsPbBr_3$ nanowire on SiO_2 substrate, showing a small absorption peak at ~ 527 nm (2.353 eV) near the band gap. Olive trace, the PL emission spectrum of $CsPbBr_3$ nanowire on SiO_2 substrate, showing an emission at ~531 nm (2.335 eV) with a FWHM of 15 nm (66 meV).

Note2 Spatially resolved PL and propagation loss spectrum of CsPbBr$_3$ nanowire

When the nanowire is excited in a position (red circles in **Figure S6 (a-d)**), the nanowire is served as microcavity where PL signals oscillate in the microcavity and finally leak out at the two ends of the nanowire. PL signal at one end of nanowire (green circles in **Figure S6 (a-d)**) is collected while changing the excitation position from P$_0$ to P$_3$. The guided PL spectra (P$_0$ ~ P$_2$) in **Figure S6e** reveals that emitted light at nanowire ends is suppressed at high energy region (<520 nm), resulting in dissymmetrical PL line shape and red shift of emission peak compared to in-situ excited PL spectra (P$_3$). It is found that the oscillation peaks occur at the lower energy region but do not emerge at high energy region. More importantly, oscillation peaks with FWHM of 1~2 nm, occur at low energy region (>530 nm) for the guided PL. The Q factor of 185-365 can be determined from the width of oscillation peaks whose positions varied from 530 nm to 554 nm. We attribute this dissymmetrical PL shape above mentioned to re-absorption of high energy photons and F-P mode guiding of low energy photons, which can be evidenced from the propagation loss spectrum in **Figure S6f**. As a function of propagation distance, the guided PL intensity varied from exponential decay at 530 nm to nearly linear decay at 535 nm, and to almost no decay at 550 nm. That means the re-absorption loss of light guiding is significantly reduced at longer wavelength during the propagation, which suggest better light guiding efficiency.[10-11]
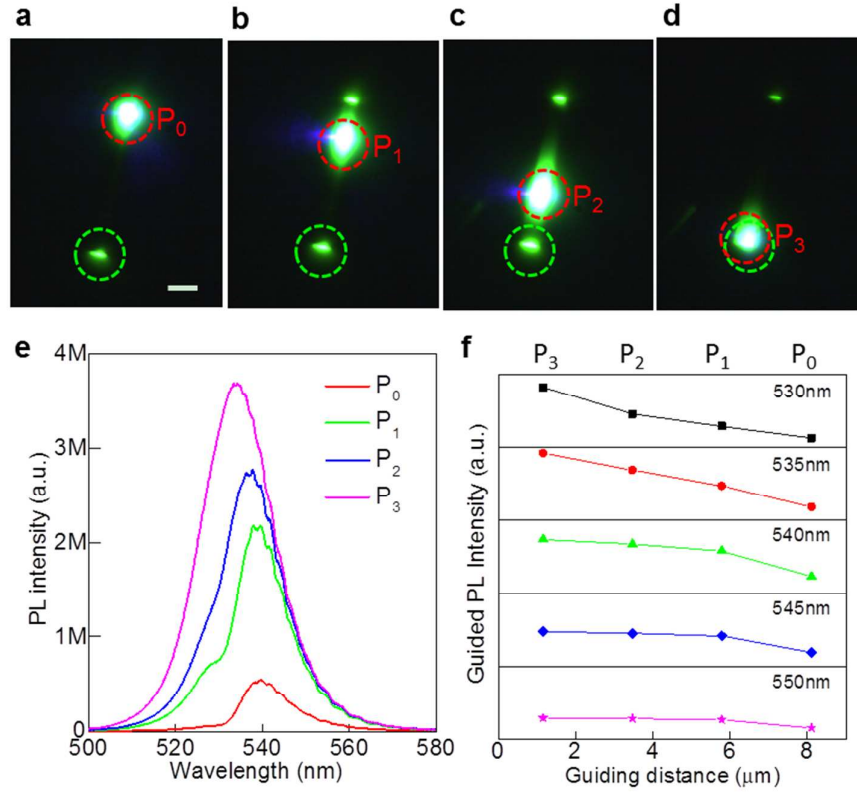
Figure S6| (a-d) Optical micrograph of the PL resulting from exciting the CsPbBr$_3$ nanowire from the upper point 0 to the end point 3 of a single nanowire outlined by red dash circle, respectively. A clear polaritonic emission spot can be seen at the both end of the CsPbBr$_3$ nanowire which is caused by guiding from the exciting point. The error bar is 2 um. **(e)** Spatially resolved PL spectra those were collected at the lower tip of CsPbBr$_3$ nanowire outlined by green dash circle as the (a-d) show. **(f)** Decay of the guided PL intensity at different wavelengths as a function of the guiding distance.

Note3 Confirmation of Fabry-Pérot cavity mode

For a Fabry-Pérot (F-P) cavity of length L, the mode spacing ($\Delta\lambda$) at λ is given by $\Delta\lambda = (\lambda^2/2L)[n - \lambda(dn/d\lambda)]^{-1}$, where n is the refractive index and $dn/d\lambda$ is the dispersion relation.[12] The group refractive index of $[n - \lambda(dn/d\lambda)]$ for light that travels at least a round trip was decided by $[n - \lambda(dn/d\lambda)] = (\lambda^2/2\Delta\lambda L)$ on the basis of F-P resonant modes of single nanowires with different length.

CsPbBr$_3$ nanowires with different lengths were measured to study the relationship between the FP-type resonance modes and the size of the nanowire microcavity. As shown in **Figure S7 (a)**, the guided PL spectra emission present an increasing number of interference peaks with increasing cavity length in the nanowire resonators. For different nanowires, the mode spacing versus *1/L* at the identical energy position is plotted in **Figure S7 (b)**, which can be linearly fitted, confirming the F-P micro cavity along the nanowire length. We notice that the slope at high energy region is smaller, indicating smaller mode spacing, which can be explained by the increasing group refractive index.
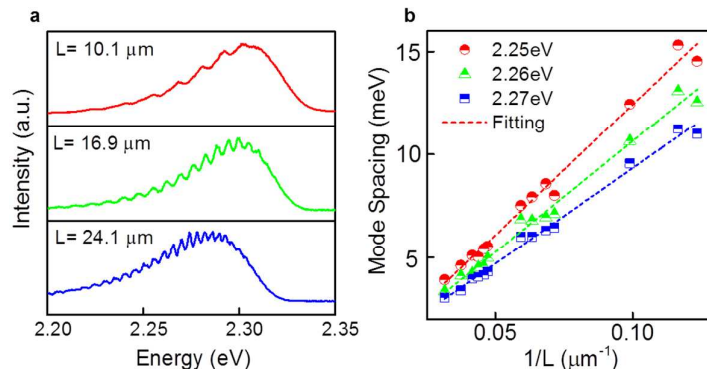

Figure S7| **(a)** Guided PL spectra collected of three CsPbBr$_3$ nanowires with different lengths. **(b)** Plot of the mode spacing at 2.25 eV, 2.26 eV, 2.27 eV as a function of 1/L. The mode spacing changes linearly with the inverse of the nanowire length.

Note4 Fitting of exciton binding energy

The exciton binding energy can be fitted using equations, [13-14] $I(T) = R\left[1 - exp\left(-\frac{E_b}{k_B T}\right)\right] + c$, where $I(T)$ is the integrated PL intensity at a specific temperature T. Therefore, temperature-dependent steady-state PL spectroscopy is conducted on individual $CsPbBr_3$ nanowire in a backscattering configuration with an excitation laser of 405 nm. The temperature is varied from 178 K to 298 K. The integrated PL intensity I_T versus T is plotted in **Figure S8** (solid black dots), showing the exciton binding energy of 40±5 meV. This value is really higher than the thermal disturbance at room temperature (KT~ 26 meV).
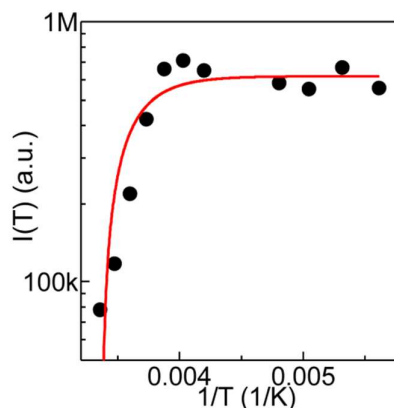

Figure S8| The integrated PL intensity I (T) as a function of $1/T$. The experimental data (black solid dots) are well fitted.

Note5 Exciton-polariton model and fitting of the dispersion curve

Because the strong coupling between excitons and photons in exciton-polaritons, the dielectric function of the coupled oscillator model can be given by:[15]

$$\varepsilon(\omega) = \varepsilon_b \left(1 + \frac{f}{\omega_T^2 - \omega^2 - i\omega\gamma} \times \frac{Ne^2}{\varepsilon_b m_e}\right),$$ where ε_b is the background dielectric constant, f is oscillator strength, γ is the exciton damping, $\frac{Ne^2}{\varepsilon_b m_e}$ is a constant connected with the material which can also be expressed as $\frac{Ne^2}{\varepsilon_b m_e} f = \omega_L^2 - \omega_T^2$, where ω_T and ω_L are the transverse and longitudinal resonance frequencies of exciton. The correspongding bulk parameters are determined as below: ε_b, $\hbar\gamma = 6.5 \times 10^{-2} \, eV$ [16] and $\hbar\omega_T = 2.365 \, eV$ are taken from literature value. We fit the measured dispersions curve by optimizing one parameter $\hbar\omega_L$. Exciton spatial dispersion is neglected since the upper polariton branche (UPB) is severely damped and only modes on the lower polariton branch (LPB) exist.[17]

Note6 Numerical calculations of coupling strength

The coupling strength is expressed as the Rabi frequency: [18]

$$g = \sqrt{\frac{e^2}{4\varepsilon_0 \varepsilon_r m_0} \frac{n(V) * f(V)}{V_{eff}(V)}} \qquad (S1)$$

with $n(V)$ the number of oscillators, $f(V)$ the oscillator strength, $V_{eff}(V)$ the effective mode volume. The oscillator strength can be expressed as (from **Note5**):

$$f = (\omega_L^2 - \omega_T^2) \cdot \frac{\varepsilon_b \varepsilon_0 m}{Ne^2} \qquad (S2)$$

Here N is the number of oscillators per unit volume; m represents the electron mass.

$1/N$ is the volume of unit cell Ω.[19] Since CsPbBr$_3$ crystallize in the cubic symmetry in our work, the unit cell volume is $\Omega = a^3$, where $a = 5.874\,\text{Å}$ [20] is the lattice constant. The value of oscillator strength for each nanowire can be obtained after determining the value of ω_L. By putting equation S2 into equation S1, Rabi frequency can be expressed as

$$g = \sqrt{\frac{(\omega_L^2 - \omega_T^2) \cdot V}{4V_{eff}}} \qquad (S3)$$

For bulk cavities, using the approximation, $\omega_L^2 - \omega_T^2 \approx 2\omega_0(\omega_L - \omega_T) = 2\omega_0\omega_{LT}$, $V_{eff} \approx V$, the Rabi frequency can be expressed as

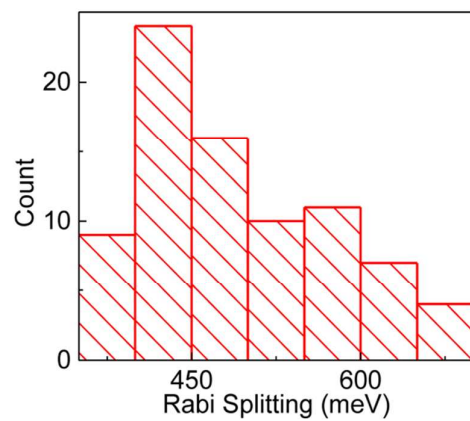$$g_{bulk} = \sqrt{\frac{\omega_0\omega_{LT}}{2}} \qquad (S4).$$

Figure S9| A histogram showing the Rabi splitting energy for almost one hundred nanowires

Note7 Mode simulation and effective volume of CsPbBr$_3$ nanowire waveguide

Eigenmode solver (MODE solutions, Lumerical Inc.) was utilized to simulate the waveguide mode in CsPbBr$_3$ nanowires with triangle cross-section lying on SiO$_2$ substrate. The simulation with the mesh step set to be 10 nm contained a perfectly matched layer (PML) boundary condition at a distance of 3λ from the nanowire surface. The calculated wavelength is set at 540 nm where polarition emission peaks usually occur. The refractive index of CsPbBr$_3$ at 540 nm (2.3) is taken from literature value.[20] The width (W) and height (H) of nanowires vary from each other. We choose the ratio of $W/H = 2.4$ in this simulation which was obtained from the AFM data. The sustainable waveguide modes in this nanowire waveguide are not well defined transverse electric (TE) or transverse magnetic (TM) modes. They are all TE-like with a certain longitudinal component.

Since the length of the nanowires is much longer than the lateral dimensions, the effective volume of CsPbBr$_3$ nanowires can be obtained by numerically calculating the electric field intensity E^2 disreibution of the cross-section region by [18]

$$
\begin{aligned}
V_{eff} &= \frac{\int_{Vs} \varepsilon(r)|E(r)|^2 \, d^3r}{\int_{V} \varepsilon(r)|E(r)|^2 \, d^3r} \cdot V \\
&= L \cdot \frac{\int_{As} \varepsilon(x,y)|E(x,y)|^2 \, dxdy}{\int_{A} \varepsilon(x,y)|E(x,y)|^2 \, dxdy} \cdot A
\end{aligned}
\tag{S5}
$$

Here $V_s(A_s)$ is the simulation volume (area), $V(A)$ is the geometric volume (cross-section area) of nanowire.
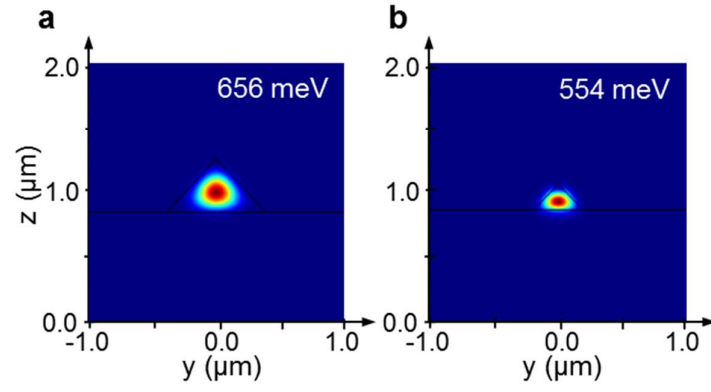
Figure S10| Normalized electric field distribution $|E|^2$ for two nanowire diameters, showing that the smaller one exits the leakage of electric field to the surrounding.

Note8 Group index of a CsPbBr$_3$ nanowire modeled with different coupling strength

The change of group index reflects the curvature of dispersion curve in the same energy region. The dispersion property of perovskite nanowire microcavity consists of two elements- material dispersion and waveguide dispersion, where the former one is explained as the strong light-matter coupling. If there is no strong exciton-photon coupling, which means no change of refractive index in material dispersion (based on the present coupled oscillator model of dielectric function). For a certain nanowire in the manuscript (**Figure 2d** and **2h**), a typical comparison of group index modeled with different value of longitudinal-transverse splitting E_{LT} ($E_{LT} = \hbar\omega_L - \hbar\omega_T$, a quantity which is proportional to Rabi splitting energy) is shown in **Figure S11**. As E_{LT} decreases from 91 meV to 1 meV, the group index also reduces from 23 to 2.7 at shorter wavelength, and from 3.6 to 2.5 at longer wavelength. When E_{LT} is zero, *i.e.,* no exciton-photon coupling, the group index varies from 2.42 to 2.45 in the studied range of wavelength, noting that the refractive index of CsPbBr$_3$ is 2.3. The slight change of group index at different wavelength is induced by the waveguide dispersion, as is mentioned above.
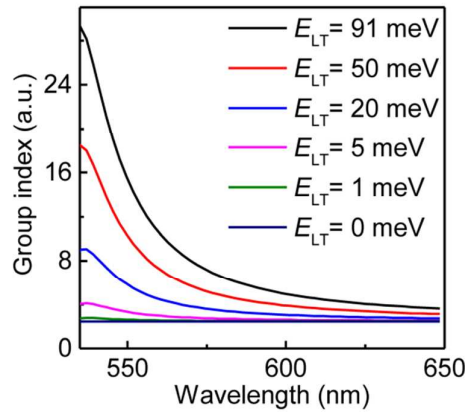
Figure S11| Group index of a CsPbBr$_3$ nanowire modeled with different value of longitudinal-transverse splitting E_{LT}

Note9 Temperature-dependent study of Rabi splitting energy

We have conducted the temperature-dependent spatially resolved PL measurement. The modulated PL spectra of a CsPbBr$_3$ nanowire at different temperature from 130 K to 293 K are exhibited in **Figure S12a**. The line width of the guided spectrum is found to be narrowed with the decrease of temperature and the peaks of the guided PL spectrum (black arrow line) and the in-situ PL spectrum (red arrow line) are moving to the opposite direction as the temperature changes. As we know, the exciton damping γ and the transverse resonance frequency of exciton ω_t in our coupled oscillator model are determined by the line width of absorption spectrum and the exciton energy which are varied with temperature according to the above result and the reference. [5] Energy-wavevector dispersion curves (scatter) determined from the modulated PL spectra are shown in **Figure S12b**. Fitting the measured dispersion curves by the parameters varied with temperature, LPB of exciton-polariton dispersion curves are obtained (the solid lines in **Figure S12b**). Fitting result of Rabi splitting for different temperatures from 170 K to 293 K dramatically increased from 406 to 496 meV. Hence, we draw the conclusion that the Rabi splitting energy changes with temperature.
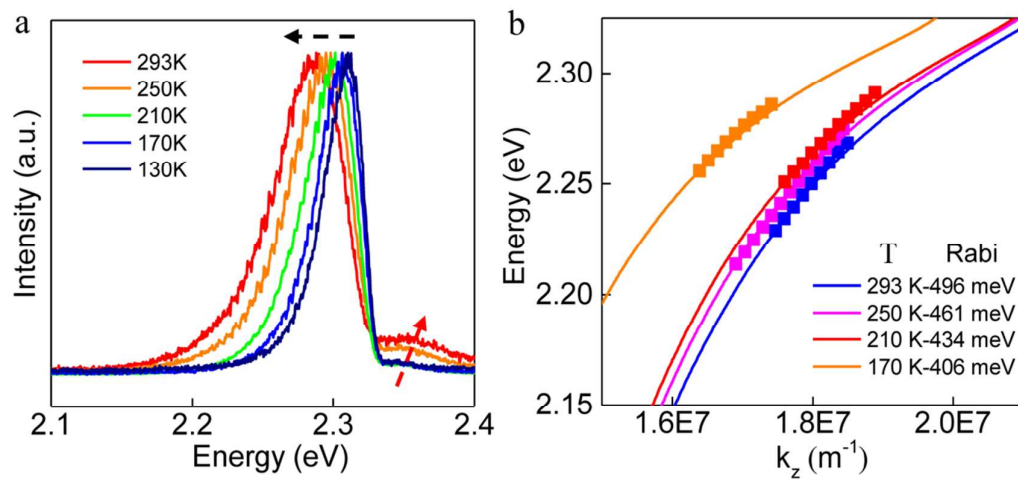
Figure S12 **(a)** The temperature-dependent spatially resolved PL spectra and **(b)** the corresponding energy-wavevector dispersion curves.

Note10 Power dependent lasing energy blueshift

We plot lasing spectra with each mode labeled number of two nanowires with different Rabi splitting energy and the corresponding blueshift of each lasing mode with the increase of pump fluence of two nanowires. For both nanowires and all modes, a blueshift is observed from the **Figure S13**. This contrasts with conventional laser frequency pulling where the emission shifts towards the gain maximum. [21] The observed power-dependent blueshift is a clear signature of polariton–polariton and polariton–exciton interactions. [22] In addition, the blueshift of lasing modes for the nanowire with larger Rabi splitting energy (554 meV) exhibits a reduced blueshift, comparing with those with smaller Rabi splitting energy (357 meV). The slow blueshift is in agreement with its lower threshold shown in **Figure 5**.
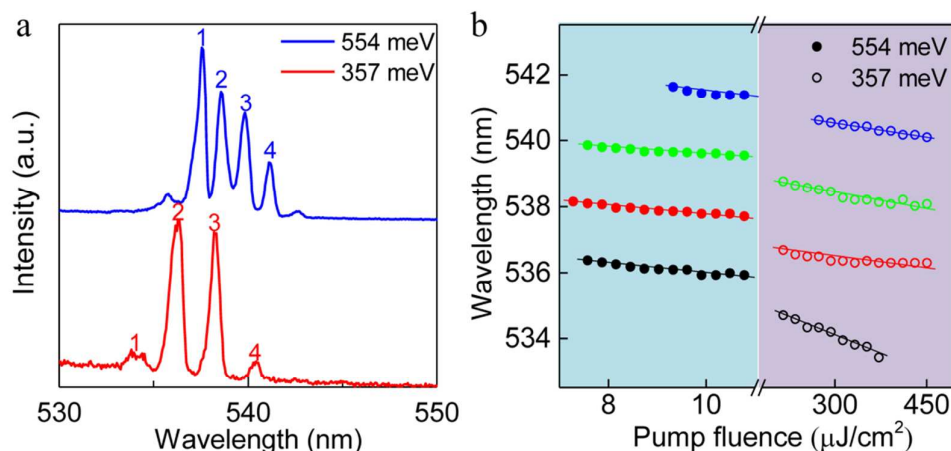

Figure S13| **(a)** Lasing modes labeled number of two nanowires with different Rabi splitting energy. **(b)** The blueshift of each lasing mode with the increase of pump fluence of two nanowires.

Table 1 Oscillator strengths of different semiconductor materials

Materials	Morphology	oscillator strength	lateral dimension	Ref.
ZnO	bulk	2.6×10^{-3} , 5.2×10^{-3}	0.7μm	23
	nanofibre	17.21	4 nm	24
CdS	bulk	0.00256	1.5 mm	25
	nanocluster	0.1472	1.28 nm	25-26
CsPbBr$_3$	nanoplatelets	1.18×10^4	14.8-20.2 nm	27

References:

(1) Sharma, S.; Weiden, N.; Weiss, A., Phase-Diagrams of Quasi-Binary Systems of the Type - Abx3-A'bx3 Abx3-Ab'x3, and Abx3-Abx'3 X = Halogen. *Z. Phys. Chem.* **1992,** *175*, 63-80.

(2) Protesescu, L.; Yakunin, S.; Bodnarchuk, M. I.; Krieg, F.; Caputo, R.; Hendon, C. H.; Yang, R. X.; Walsh, A.; Kovalenko, M. V., Nanocrystals of Cesium Lead Halide Perovskites (CsPbX(3), X = Cl, Br, and I): Novel Optoelectronic Materials Showing Bright Emission with Wide Color Gamut. *Nano Lett.* **2015,** *15*, 3692-6.

(3) Li, X.; Wu, Y.; Zhang, S.; Cai, B.; Gu, Y.; Song, J.; Zeng, H., CsPbX3 Quantum Dots for Lighting and Displays: Room-Temperature Synthesis, Photoluminescence Superiorities, Underlying Origins and White Light-Emitting Diodes. *Adv. Funct. Mater.* **2016,** *26*, 2435-2445.

(4) Zhou, H.; Yuan, S.; Wang, X.; Xu, T.; Wang, X.; Li, H.; Zheng, W.; Fan, P.; Li, Y.; Sun, L.; Pan, A., Vapor Growth and Tunable Lasing of Band Gap Engineered Cesium Lead Halide Perovskite Micro/Nanorods with Triangular Cross Section. *ACS Nano* **2017,** *11*, 1189-1195.

(5) Zhang, Q.; Su, R.; Liu, X.; Xing, J.; Sum, T. C.; Xiong, Q., High-Quality Whispering-Gallery-Mode Lasing from Cesium Lead Halide Perovskite Nanoplatelets. *Adv. Funct. Mater.* **2016,** *26*, 6238-6245.

(6) Fu, Y.; Zhu, H.; Stoumpos, C. C.; Ding, Q.; Wang, J.; Kanatzidis, M. G.; Zhu, X.; Jin, S., Broad Wavelength Tunable Robust Lasing from Single-Crystal Nanowires of Cesium Lead Halide Perovskites (CsPbX3, X = Cl, Br, I). *ACS Nano* **2016,** *10*, 7963-7972.

(7) Ravi, V. K.; Markad, G. B.; Nag, A., Band Edge Energies and Excitonic Transition Probabilities of Colloidal CsPbX3 (X = Cl, Br, I) Perovskite Nanocrystals. *ACS Energy Lett.* **2016,** *1*, 665-671.

(8) Zhang, D. D.; Yang, Y. M.; Bekenstein, Y.; Yu, Y.; Gibson, N. A.; Wong, A. B.; Eaton, S. W.; Kornienko, N.; Kong, Q.; Lai, M. L.; Alivisatos, A. P.; Leone, S. R.; Yang, P. D., Synthesis of Composition Tunable and Highly Luminescent Cesium Lead Halide Nanowires through Anion-Exchange Reactions. *J. Am. Chem. Soc.* **2016,** *138*, 7236-7239.

(9) Akkerman, Q. A.; Motti, S. G.; Kandada, A. R. S.; Mosconi, E.; D'Innocenzo, V.; Bertoni, G.; Marras, S.; Kamino, B. A.; Miranda, L.; De Angelis, F.; Petrozza, A.; Prato, M.; Manna, L., Solution Synthesis Approach to Colloidal Cesium Lead Halide Perovskite Nanoplatelets with Monolayer-Level Thickness Control. *J. Am. Chem. Soc.* **2016,** *138*, 1010-1016.

(10) Piccione, B.; van Vugt, L. K.; Agarwal, R., Propagation loss spectroscopy on single nanowire active waveguides. *Nano Lett.* **2010,** *10*, 2251-6.

(11) Zhang, C.; Zou, C. L.; Yan, Y.; Hao, R.; Sun, F. W.; Han, Z. F.; Zhao, Y. S.; Yao, J., Two-photon pumped lasing in single-crystal organic nanowire exciton polariton resonators. *J. Am. Chem. Soc.* **2011,** *133*, 7276-9.

(12) O'Carroll, D.; Lieberwirth, I.; Redmond, G., Microcavity effects and optically pumped lasing in single conjugated polymer nanowires. *Nat. Nanotechnol.* **2007,** *2*, 180-184.

(13) Chen, Z.; Yu, C.; Kai, S.; Wang, J. J.; Pfenninger, W.; Vockic, N.; Midgley, J.; Kenney, J. T., Photoluminescence study of polycrystalline CsSnI 3 thin films: Determination of exciton binding energy. *J. Lumin.* **2012,** *132*, 345-349.

(14) Zhang, Q.; Ha, S. T.; Liu, X.; Sum, T. C.; Xiong, Q., Room-Temperature Near-Infrared High-Q Perovskite Whispering-Gallery Planar Nanolasers. *Nano Lett.* **2014,** *14*, 5995-6001.

(15) van Vugt, L. K., Optical properties of semiconducting nanowires. *PhD thesis* **2007**.

(16) Kunugita, H.; Hashimoto, T.; Kiyota, Y.; Udagawa, Y.; Takeoka, Y.; Nakamura, Y.; Sano, J.; Matsushita, T.; Kondo, T.; Miyasaka, T.; Ema, K., Excitonic Feature in Hybrid Perovskite CH3NH3PbBr3Single Crystals. *Chem. Lett.* **2015,** *44*, 852-854.

(17) van Vugt, L. K.; Piccione, B.; Agarwal, R., Incorporating polaritonic effects in semiconductor nanowire waveguide dispersion. *Appl. Phys. Lett.* **2010,** *97*, 061115.

(18) van Vugt, L. K.; Piccione, B.; Cho, C.-H.; Nukala, P.; Agarwal, R., One-dimensional polaritons with size-tunable and enhanced coupling strengths in semiconductor nanowires. *Proc. Natl. Acad. Sci. USA* **2011,** *108*, 10050-10055.

(19) Klingshirn, C. F., Ensemble of Uncoupled Oscillators. In *Semiconductor Optics*, Springer Berlin Heidelberg: Berlin, Heidelberg, 2012; pp 77-95.

(20) Park, K.; Lee, J. W.; Kim, J. D.; Han, N. S.; Jang, D. M.; Jeong, S.; Park, J.; Song, J. K., Light-Matter Interactions in Cesium Lead Halide Perovskite Nanowire Lasers. *J. Phys. Chem. Lett.* **2016,** *7*, 3703-3710.

(21) Daskalakis, K. S.; Maier, S. A.; Murray, R.; Kena-Cohen, S., Nonlinear interactions in an organic polariton condensate. *Nat. Mater.* **2014,** *13*, 271-8.

(22) Su, R.; Diederichs, C.; Wang, J.; Liew, T. C. H.; Zhao, J.; Liu, S.; Xu, W.; Chen, Z.; Xiong, Q., Room-Temperature Polariton Lasing in All-Inorganic Perovskite Nanoplatelets. *Nano Lett.* **2017,** *17*, 3982-3988.

(23) Lagois, J.; Hümmer, K., Experimental and theoretical effects of surface layers and spatial dispersion on the free exciton reflectance of ZnO. *Phys. Status Solidi* **2010,** *72*, 393-402.

(24) Dallali, L.; Jaziri, S.; Haskouri, J. E.; Amorós, P., Optical properties of exciton confinement in spherical ZnO quantum dots embedded in SiO 2 mathContainer Loading Mathjax matrix. *Superlattices & Microstructures* **2009,** *46*, 907-916.

(25) Thomas, D. G.; Hopfield, J. J., Exciton Spectrum of Cadmium Sulfide. *Phys. Rev.* **1959,** *116*, 573-582.

(26) Vossmeyer, T.; Katsikas, L.; Giersig, M.; Popovic, I. G.; Diesner, K.; Chemseddine, A.; Eychmueller, A.; Weller, H., CdS Nanoclusters: Synthesis, Characterization, Size Dependent Oscillator Strength, Temperature Shift of the Excitonic Transition Energy, and Reversible Absorbance Shift. *J. Phys. Chem.* **1994,** *98*, 7665-7673.

(27) Li, J.; Luo, L.; Huang, H.; Ma, C.; Ye, Z.; Zeng, J.; He, H., 2D Behaviors of Excitons in Cesium Lead Halide Perovskite Nanoplatelets. *J. Phys. Chem. Lett.* **2017,** *8*, 1161-1168.